Journal of Physics: Conference Series

OPEN ACCESS

Damage detection strategies for aircraft shell–like structures based on propagation guided elastic waves

To cite this article: A Żak *et al* 2011 *J. Phys.: Conf. Ser.* **305** 012055

View the article online for updates and enhancements.

You may also like

- Multi-sinc Schell-model beams and the interaction with a linear random medium
Zhangrong Mei and Yonghua Mao
- Propagation properties of stochastic electromagnetic non-uniformly correlated partially coherent pulses in dispersive media
Chaoliang Ding, Xinxin Wang, Yongtao Zhang et al.
- Anisotropic-source-induced changes of the degree of polarization of stochastic electromagnetic beams on propagation
Hua Wang, Xiangzhao Wang, Aijun Zeng et al.

This content was downloaded from IP address 153.19.58.141 on 11/06/2024 at 12:50

Journal of Physics: Conference Series **305** (2011) 012055 doi:10.1088/1742-6596/305/1/012055

Damage detection strategies for aircraft shell–like structures based on propagation guided elastic waves

A Żak[1], **W Ostachowicz**[1,2], **M Krawczuk**[1,3]

[1] The Szewalski Institute of Fluid–Flow Machinery, Polish Academy of Sciences, Fiszera 14, 80–952 Gdańsk, Poland
[2] Gdynia Maritime University, Faculty of Navigation, Al. Zjednoczenia 3, 81–345 Gdynia, Poland
[3] Gdansk University of Technology, Faculty of Electrical and Control Engineering, Narutowicza 11/12, 80–952 Gdańsk, Poland

E–mail: a.zak@imp.gda.pl

Abstract. Damage of aircraft structural elements in any form always present high risks. Failures of these elements can be caused by various reasons including material fatigue or impact leading to damage initiation and growth. Detection of these failures at their earliest stage of development, estimation of their size and location, are one of the most crucial factors for each damage detection method. Structural health monitoring strategies based on propagation of guided elastic waves in structures and wave interaction with damage related discontinuities are very promising tools that offer not only damage detection capabilities, but are also meant to provide precise information about the state of the structures and their remaining lifetime. Because of that various techniques are employed to simulate and mimic the wave–discontinuity interactions. The use of various types of sensors, their networks together with sophisticated contactless measuring techniques are investigated both numerically and experimentally. Certain results of numerical simulations obtained by the use of the spectral finite element method are presented by the authors and related with propagation of guided elastic waves in shell–type aircraft structures. Two types of structures are considered: flat 2D panels with or without stiffeners and 3D shell structures. The applicability of two different damage detection approaches is evaluated in order to detect and localise damage in these structures. Selected results related with the use of laser scanning vibrometry are also presented and discussed by the authors.

1. Introduction

A better understanding of phenomena associated with propagation of guided elastic waves in elements of structures is very important from both the theoretical and the practical point of view. Various anomalies in wave propagation patterns in structural elements can be observed and next interpreted and employed for damage detection or identification purposes [1–5].

For this reason the development of effective numerical tools that can be successfully used for investigation of the phenomena of guided elastic wave propagation has become a very important issue.

Published under licence by IOP Publishing Ltd

MOST WIEDZY Downloaded from mostwiedzy.pl

A very well established method that enables scientists and researchers to study these phenomena is the spectral finite element method (SFEM), as proposed by Patera in 1984 [6].

The SFEM is very well suited for investigation of various elastic wave propagation problems in structures of complex geometries. This approach has its origin in the application of spectral series (Fourier or Chebyshev) for solutions of partial differential equations [7] and employs essentially the same ideas as the finite element method (FEM). Its main applications fields cover fluid dynamics [8], heat transfer [9], acoustics [10], seismology [11], and also mechanical engineering [12–17].

It is well known that the presence of damage results in reflection and scattering of propagating elastic waves and such features have been commonly used for damage detection purposes. In this work certain results of numerical simulations obtained by the use of the SFEM are presented by the authors. The applicability of two different damage detection approaches is evaluated in order to detect and localise damage in structures. Selected results related with the use of laser scanning vibrometry are also presented and discussed by the authors.

2. Spectral finite element method

In the current formulation of a spectral shell finite element the coordinates of the element nodes are defined in the local coordinate system of the element as the roots of the following polynomial expression [14–16]:

$$(1-\zeta)^2 P_n'(\zeta) = 0, \quad \zeta \in [-1,+1] \tag{1}$$

where $P_n(\zeta)$ is the $n-$th order Legendre polynomial and the symbol $'$ denotes the first derivative. In the case of the spectral shell finite element used by the authors the nodal coordinates at $n=5$ are specified as:

$$\xi_m, \eta_n \in \{-1, -\sqrt{\tfrac{1}{3}+\tfrac{2}{3\sqrt{7}}}, -\sqrt{\tfrac{1}{3}-\tfrac{2}{3\sqrt{7}}}, \sqrt{\tfrac{1}{3}-\tfrac{2}{3\sqrt{7}}}, \sqrt{\tfrac{1}{3}+\tfrac{2}{3\sqrt{7}}}, 1\}, \quad m,n = 1,\ldots,6 \tag{2}$$

On the specified nodes a set of shape functions can be built in the local coordinate system. The Lagrange interpolation function $f(\xi,\eta)$ supported on the nodes can be defined in the following manner:

$$f(\xi,\eta) = \sum_{n=1}^{6}\sum_{m=1}^{6} N_{mn}(\xi,\eta) f_{mn} = \sum_{n=1}^{6}\sum_{m=1}^{6} N_m(\xi) N_n(\eta) f_{mn}, \quad m,n = 1,\ldots,6 \tag{3}$$

where $N_m(\xi)$ and $N_n(\eta)$ are one–dimensional shape functions of the element, while f_{mn} are the nodal values of the function $f(\xi,\eta)$. The approximation shape functions $N_m(\xi)$ and $N_n(\eta)$ are orthogonal in a discrete sense:

$$\int_{-1}^{+1} N_m(\xi) N_n(\xi) d\xi = \sum_{k=1}^{6} \omega_k N_m(\xi_k) N_n(\xi_k) = \omega_{mn}\delta_{mn}, \quad k,m,n = 1,\ldots,6 \tag{4}$$

where ω_{mn} is the Gauss–Lobatto weight and δ_{mn} is the Kronecker delta [14–16].

Assuming small strains the displacement field in the mid–plane of the spectral shell finite element can be expressed in a very well–known form [17–19]. Based on the assumed displacement field the strains in the element can be expressed according to the first order shear deformation theory [20] leading to the definition of the characteristic inertia (diagonal) and stiffness matrices of the spectral element [21], as shown in [17–19].

MOST WIEDZY Downloaded from mostwiedzy.pl

3. Numerical simulations

Numerical simulations were divided into two parts. In the first part a flat square plate made out of aluminium alloy 2024–T3 was investigated, while the second part was related to a wing section skin. In both these cases propagation of guided elastic waves [17–19] was investigated by the use of the SFEM and changes in the wave propagation patterns were studied in the context of damage detection and localisation. As a source of excitation a 5 cycle sine pulse of 75 kHz modulated by Hanning window [14–16] was employed. Both the structures were modelled by 2500 shell spectral finite elements at the total number of model degrees of freedom approximately equal to 380,000. Boundary conditions of free type were considered.

In order to overcome the problems resulting from the presence of dead zones in distributed sensor networks, as presented in [22–24], it was decided to employ an approach, in which damage related maps are based on two different time integral indexes. They are calculated at selected points of the structures, these being: the integral mean value (IMV) and the root mean square (RMS). They were defined as follows:

$$\mathrm{IMV}[s] = \frac{1}{t_2 - t_1}\int_{t_1}^{t_2} s(t)dt \approx \frac{1}{n}\sum_{k=1}^{n} s(t_k)$$
$$t_k = t_1 + (k-1)\Delta t, \quad \Delta t = \frac{t_2 - t_1}{n-1}, \quad k = 1,2,\ldots,n \tag{5}$$

$$\mathrm{RMS}[s] = \sqrt{\frac{1}{t_2 - t_1}\int_{t_1}^{t_2} \left[s(t)\right]^2 dt} \approx \sqrt{\frac{1}{n}\sum_{k=1}^{n}\left[s(t_k)\right]^2}$$
$$\mathrm{RMS}^*[s] = \sqrt{\frac{1}{n}\sum_{k=1}^{n}\left[w_k s(t_k)\right]^2}, \quad w_k = 1,k,k^2,\ldots \tag{6}$$

where $s(t)$ denotes a response signal, n is the total number of samples in signal $s(t)$, $(t_2 - t_1)$ is the length of the sampling process, while w_k is a weighting factor that increases the influence of signal samples towards the end of the sampling process.

In practice this approach can be successfully realised by the application of laser scanning vibrometry, whereas in the current numerical study as the reference (measurement) points, used to calculate the values of the integrals (5) and (6), selected elemental nodes were taken, in which all displacement components were calculated. The total time of numerical simulations covered 0.5 ms in each case investigated, however, the IMV and RMS damage maps were calculated for various lengths of sampling processes in order to reveal the influence of signal reflections and mode conversion, assuming $t_1 = 0$.

The IMV and RMS damage maps obtained and based on the results of numerical simulations for the square aluminium plate (500 mm × 500 mm × 1 mm) are presented in Fig. 1 and Fig. 2. They were calculated for the force excitation of 10 N acting transversely and located at the plate centre. The maps were plotted for all three displacement components and as damage an additional mass of 2.5 g was assumed placed on the plate surface. In the maps dark areas correspond to greater values of the IMV and RMS integral values, while white light areas correspond to their smaller values.

It can be clearly seen from the results presented in Fig. 1 and Fig. 2 that both the IMV and RMS damage maps can indicate clearly the location of the additional mass. This is true for all displacement components investigated, however, in the case of the RMS damage map the position of the mass is more clearly visible. It is interesting to note that the use of the in–plane displacement components results in better sensitivity in both cases, however, from a practical point of view measurements of the in–plane displacement components by scanning laser vibrometry is more difficult. Because of that only the transverse displacement component was taken into consideration in all the following results

MOST WIEDZY Downloaded from mostwiedzy.pl

presented. It should be pointed out that due to the 2–D nature of the plate the IMV and RMS damage maps are virtually based on the behaviour of A_0 Lamb wave mode only that is dominating in the current case.

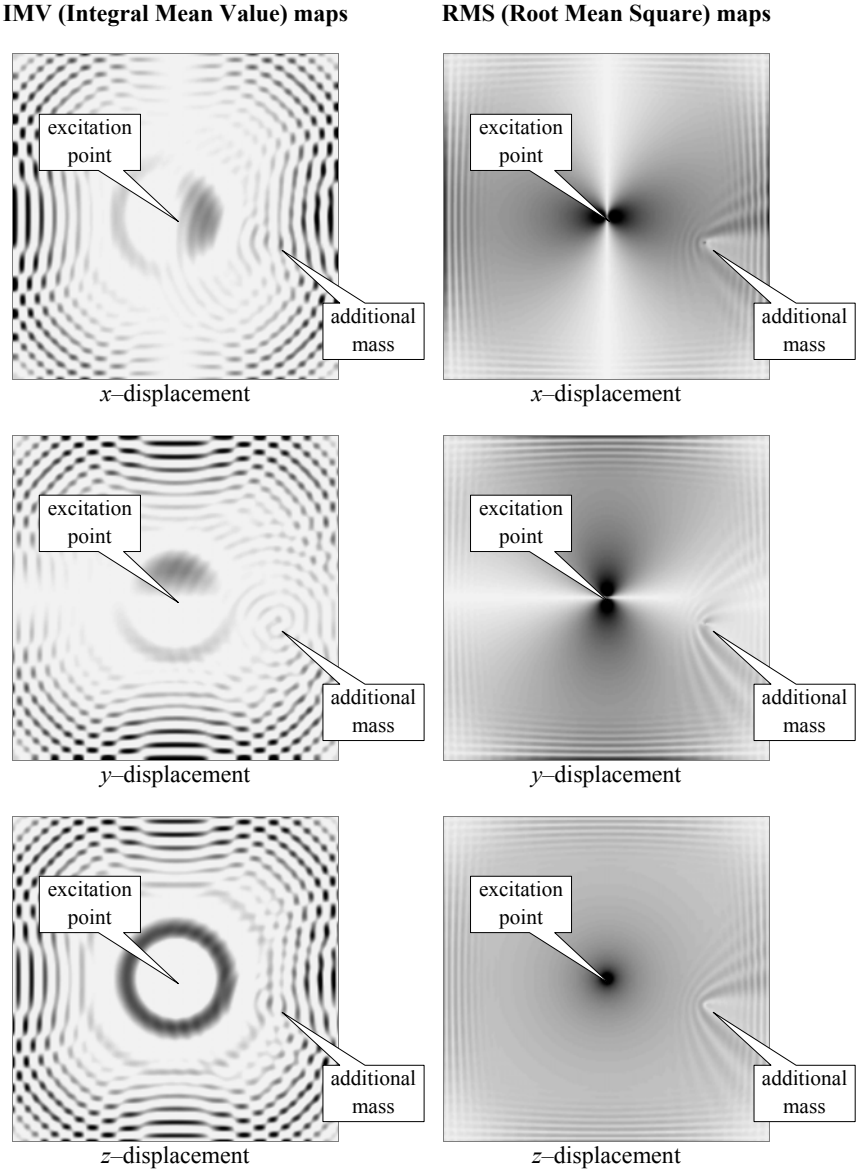

Figure 1. IMV damage maps based on results of numerical simulation by the spectral finite element method – additional mass of 2.5 g placed on an aluminium plate ($t_2 - t_1 = 0.5$ ms).

Figure 2. RMS damage maps based on results of numerical simulation by the spectral finite element method – additional mass of 2.5 g placed on an aluminium plate ($t_2 - t_1 = 0.5$ ms).

Results of numerical simulations shown in Fig. 3 and Fig. 4 are related to RMS damage maps. It can be seen from the results presented in Fig. 3 that the total length of the sampling processes, or the signal length that is considered in calculation of the integral (6), has a great influence on the resulting RMS damage maps. Longer signals employed for computations lead to better map resolutions, however, for very long signals strong influence resulting from structural boundary reflections may be

MOST WIEDZY Downloaded from mostwiedzy.pl

visible. This may mask damage of small sizes, especially in the case of their proximity to the boundaries and relatively high signal noise.

It should be mentioned that the resolution of the RMS damage maps can be enhanced by the use of various weighting factors, as presented in Fig. 4. The application of the weighting factors helps to improve the map sensitivity to small size defects that are distant from the excitation points by increasing their importance on the time scale. In this case much shorter time signals may be employed in order to calculate the integral (6) in comparison to the original signal lengths. This technique may be also applied when structural damping is strong, which results in strong signal attenuation.

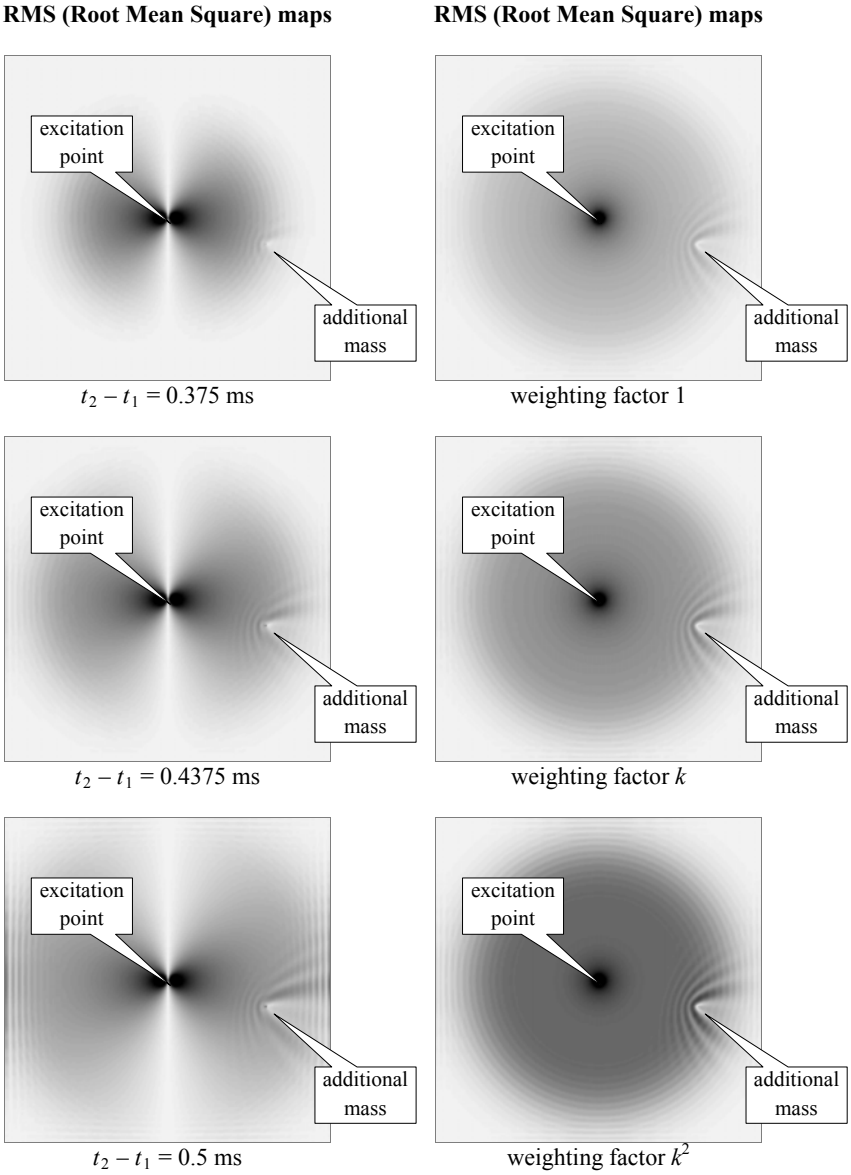

Figure 3. Influence of the signal length on RMS damage maps for x–displacement component based on results of numerical simulation by the spectral finite element method – detection of an additional mass of 2.5 g placed on an aluminium plate.

Figure 4. Influence of the weighting factor on RMS damage maps for z–displacement component based on results of numerical simulation by the spectral finite element method – detection of an additional mass of 2.5 g placed on an aluminium plate ($t_2 - t_1$ = 0.375 ms).

MOST WIEDZY Downloaded from mostwiedzy.pl

The following two examples of numerical simulations illustrate the influence of the weighting factors on RMS damage maps in the case of a wing section skin (500 mm × 250 mm × 1 mm). Dynamic responses of the structure were calculated in this case for the force excitation of 10 N acting transversely and located at the edge.

Two damage scenarios were investigated here: first in the form of additional mass of 2.5 g and second in the form of small and open crack (10 mm long). In both these cases only the transverse displacement component was taken into account. It should be stressed here that contrary to the case of the flat plate and due to the 3–D nature of the structure the RMS damage maps carry information on the multimode behaviour of propagating Lamb wave modes (A_0, S_0, and SH_0) and their coupled interaction with damage. This greatly improves the sensitivity of the current approach to damage of various types, but on the other hand results in much more complicated patterns that can be obtained.

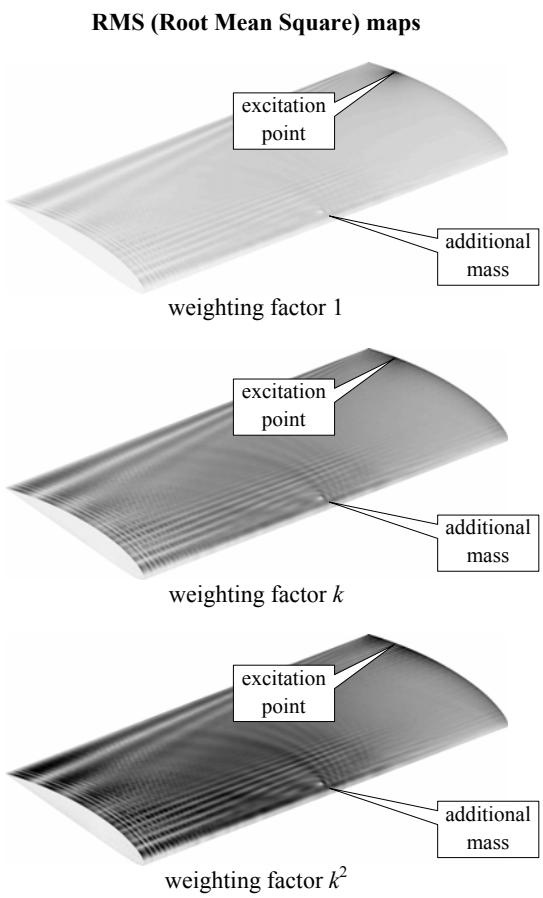

Figure 5. Influence of the weighting factor on RMS damage maps for z–displacement component based on results of numerical simulation by the spectral finite element method – detection of an additional mass of 2.5 g placed on an aluminium wing section skin ($t_2 - t_1 = 0.375$ ms).

Figure 5 illustrates the influence of the weighting factor on RMS damage maps for the transverse displacement component used for detection of the additional mass of 2.5 g, while results presented in Fig. 6 correspond to detection of the open crack. In the case of the additional mass the RMS damage map calculated for the weighting factor k reveals the presence of the damage, while for the weighting factor k^2 the damage is very well visible. In the case of the open crack, because of the greater magnitude of the damage and its orientation in respect to the front of the waves propagating from the excitation point.

MOST WIEDZY Downloaded from mostwiedzy.pl

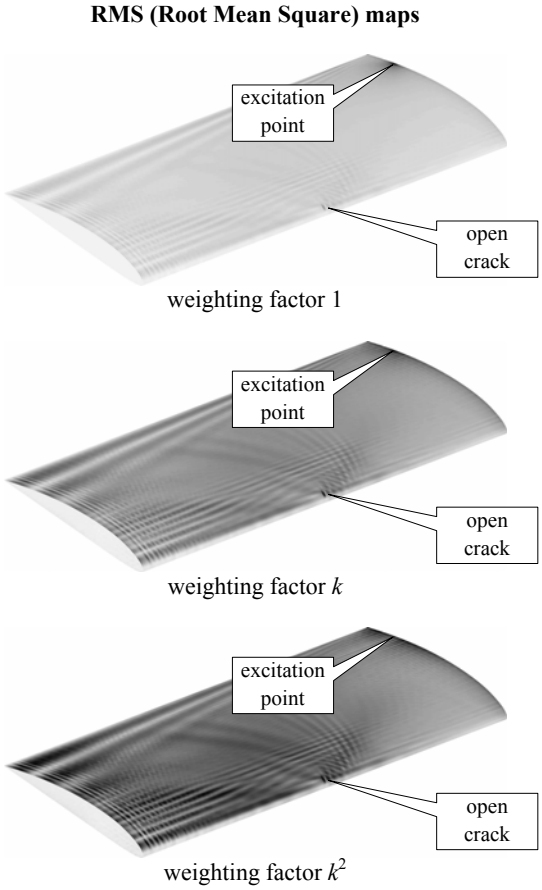

Figure 6. Influence of the weighting factor on RMS damage maps for z–displacement component based on results of numerical simulation by the spectral finite element method – detection of an open crack in an aluminium wing section skin ($t_2 - t_1$ = 0.375 ms).

4. Experimental investigation

In order to verify the approach discussed a series of experimental measurements were performed on the composite stabiliser of a PZL W–3A helicopter shown in Fig. 7. The measurements were carried out by the use of a 3–D laser scanning vibrometry unit Polytec PSV–400–3D. A general view of the scanning vibrometry unit is presented in Fig. 8. As excitation signals, generated by a Sonox® CeramTec PZT element of 10 mm diameter, 5 cycle sine pulses of 35 kHz or 100 kHz modulated by Hanning [14–16] window were employed.

Measurements were carried out on in a rectangular area of 845 mm × 510 mm, in which a matrix of 475 × 291 measurement points was selected. Each measurement was repeated 20 times and the results obtained in this way were averaged in order to improve accuracy. A single measurement event covered 2 ms for 35 kHz excitation and 0.8 ms for 100 kHz excitation with an appropriate time delay between each subsequent measurement. In order to reduce the noise level and due to the geometry of the stabiliser only the transverse displacement component was considered to calculate RMS damage maps, while damage was simulated by additional elements (small metal plates or coins) glued to its top surface. Totally 7 locations were chosen for that purpose.

The results of experimental measurements confirmed those obtained from numerical simulations in the context of the applicability of the RMS integral index and its potential for damage detection and localisation in structural elements. As can be seen from Fig. 9 the RMS damage map revealed not only true locations of 6 simulated failures out of 7, but also offers an insight into the interior of the structure. This effect is even more prominent in the case of the higher excitation frequency of 100

MOST WIEDZY Downloaded from mostwiedzy.pl

kHz, as presented in Fig. 10. In this case all failures were successfully detected. It is interesting to note that higher excitation frequencies result in improved resolution and sensitivity to damage in comparison with low excitation frequencies, but smaller inspection areas.

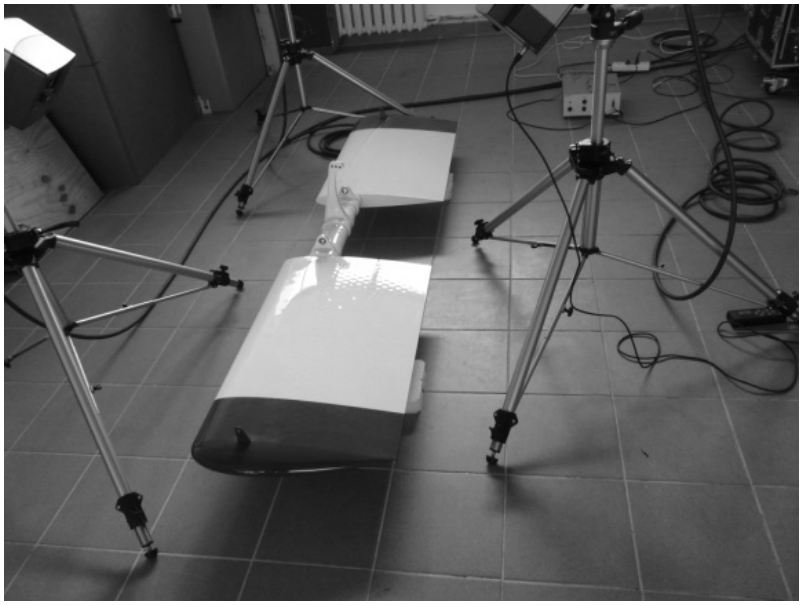

Figure 7. Composite stabiliser of a PZL W–3A helicopter used for experimental measurements and verification.

Figure 8. Polytec PSV–400–3D laser scanning vibrometry unit used for experimental tests.

MOST WIEDZY Downloaded from mostwiedzy.pl

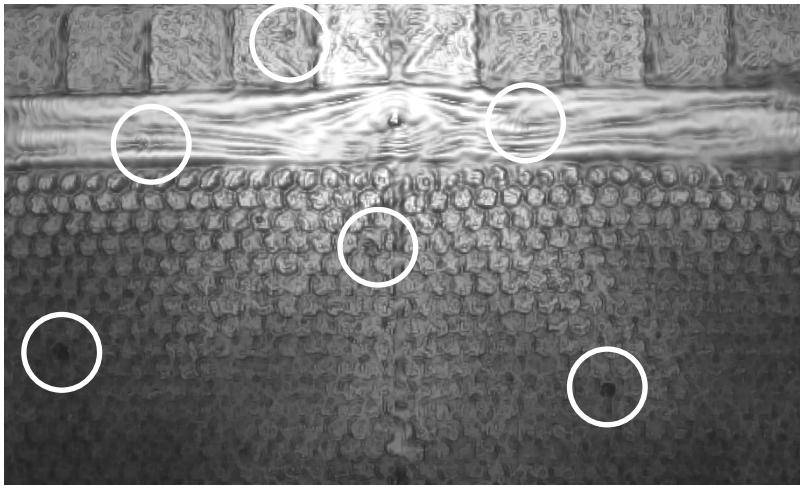

Figure 9. RMS damage maps based on results of experimental measurements by scanning laser vibrometry of the composite stabiliser of a PZL W–3A helicopter – excitation signal of 35 kHz (damage positions indicated by white circles).

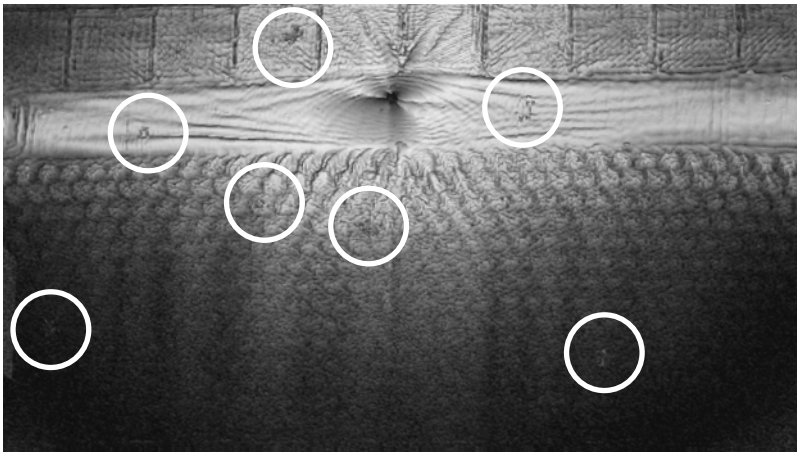

Figure 10. RMS damage maps based on results of experimental measurements by scanning laser vibrometry of the composite stabiliser of a PZL W–3A helicopter – excitation signal of 100 kHz (damage positions indicated by white circles).

5. Conclusions

Based on the results of numerical and experimental measurement it can be concluded that damage maps based on the application of integral indexes can be successfully employed in damage detection and localisation in structural elements. Out of two such indexes assessed by the authors the RMS index is more sensitive to damage than the IMV index, as well as is much less sensitive to noise. In the case of the of composite materials, were propagating guided waves are strongly attenuated, results obtained by the use of the RMS index can be improved by appropriate signal weighting process. The weighting process also offers improved detection and localisation of damage distant from the excitation point as well as located close to structural boundaries.

6. Acknowledgements

The authors of this work would like to gratefully acknowledge the support for this research provided by the Polish Ministry of Science and Higher Education through the European Funds System under the Sectoral Operational Programme Improvement of the Competitiveness of Enterprises via MONIT

MOST WIEDZY Downloaded from mostwiedzy.pl

project (Monitoring of Technical State of Construction and Evaluation of Its Lifespan) nr POIG.01.01.02–00–013/08.

6. References

[1] Chang F K 2001 Structural Health Monitoring
[2] Lakshmanan K A and Pines D J 1997 *SPIE Smart Structures and Materials* **3041** 408
[3] Palacz M and Krawczuk M 2002 *Computers and Structures* **80** 1809
[4] Krawczuk M 2002 *Finite Elements in Analysis and Design* **38** 537
[5] Ostachowicz W, Krawczuk M, Cartmell M P and Gilchrist M 2002 *Structural Health Monitoring Conference* 344
[6] Patera T 1984 *Journal of Computational Physics* **54** 468
[7] Boyd J P 1989 Cheybyshev and Fourier Spectral Methods
[8] Canuto C, Hussaini M Y, Quarteroni A and Zang T A 1989 Spectral Methods in Fluid Dynamics
[9] Spall R 1995 *International Journal of Heat Mass Transfer* **15** 2743
[10] Dauksher W and Emery A F 1996 *Review of Progress in Quantitative Non–destructive Evaluation* 97
[11] Seriani G 1998 *Computational Methods Applied in Mechanical Engineering* **164** 235
[12] Wilcox P D 2003 *IEEE Transactions on Ultrasonics, Ferroelectrics, and Frequency Control*, **50** 699
[13] Giurgiutiu V and Bao J J 2004 *Structural Health Monitoring Conference* 121
[14] Żak A, Krawczuk M and Ostachowicz W 2006 *Finite Elements in Analysis and Design* **42** 929
[15] Żak A, Krawczuk M and Ostachowicz W 2006 *Finite Elements in Analysis and Design* **46** 145
[16] Ostachowicz W, Krawczuk M, Żak A and Kudela P 2006 *Computer Assisted Mechanics and Engineering* **13** 109
[17] Żak A, Krawczuk M, Ostachowicz W, Kudela P and Palacz M 2006 *Structural Health Monitoring Conference* 316
[18] Żak A 2009 *Finite Elements in Analysis and Design*, **45** 650
[19] Żak A, Krawczuk M and Ostachowicz W 2010 *Structural Health Monitoring Conference* 2010 1031
[20] Reddy J N 1993 An Introduction to the Finite Element Method
[21] Zienkiewicz O C 1989 The Finite Element
[22] Wandowski T, Malinowski P and Ostachowicz W 2009 *Key Engineering Materials* **413–414** 87
[23] Ostachowicz W, Wandowski T and Malinowski P 2010 *SPIE* **7650** doi:10.1117/12.846911
[24] Wandowski T, Malinowski P and Ostachowicz W 2010 *Structural Health Monitoring Conference 2010* 704

MOST WIEDZY Downloaded from mostwiedzy.pl